Dynamic Analysis of Outer and Inner Race Defects on Thermoplastic Rolling Bearing System Using Implicit Finite Element Method

Nesrine Gaaliche

Unit of Mechanical Production Engineering and Materials, National School of Engineers of Sfax, Soukra Road Km 4 BP. 1173 – 3038, Sfax, Tunisia — University of Sfax.
Department of Mechanical Engineering, School of Engineering, Bahrain Polytechnic, PO Box 33349, Isa Town, Kingdom of Bahrain. E-mail nesrine.gaaliche@polytechnic.bh

Subramanian Chithambaram

Department of Mechanical Engineering, School of Engineering, Bahrain Polytechnic, PO Box 33349, Isa Town, Kingdom of Bahrain.

Raouf Fathallah

Unit of Mechanical Production Engineering and Materials, National School of Engineers of Sfax, Soukra Road Km 4 BP. 1173 – 3038, Sfax, Tunisia — University of Sfax.
National Engineering School of Sousse, BP 264 Sousse Erriadh 4023, Tunisia — University of Sousse.

(Received 11 December 2021; accepted 28 March 2022)

This paper proposes an improved finite element dynamic model to analyze the vibration response of a rolling bearing system. The vibration responses of defect free and defective polypropylene (PP) bearings are analyzed using the finite element analysis and compared with the experimental results using the in house developed bearing fatigue test rig. The boundary conditions of this model are imposed to ensure an adequate homogeneity with the experimental apparatus. This study considers the viscoelastic property of thermoplastic to investigate the effect of the flexibility and damping viscosity of material. The three-dimensional dynamic analysis detects the vibrations produced in a rolling bearing system. Modal frequencies and the vibration modes shapes which must be avoided had been determined. Monitoring the evolution of vibration signatures as a function of defect location is also carried out using Finite Element Analysis (FEM). Test results reveal that peak vibration amplitudes are more pronounced in an inner ring defect than in an outer ring defect. Vibration signals of stainless-steel bearings are investigated to compare the performance of the thermoplastic bearings with its metallic counterparts. Both test and simulation results reveal that a lower level of vibration is observed with PP bearings compared to that of metal. The PP bearings not only dampen vibrations, but also accommodate shaft misalignments unlike their steel counterparts. Once overall vibration spectrums results are validated, Von Mises stresses within the rings are evaluated under excessive loading conditions. The simulation results show that stress is high in raceways where the balls are compressed between the raceways. Computational results agree well with the experimental tests for the test scenarios.

NOMENCLATURE

F_s	shaft rotational frequency (Hz)
F_I	ball pass frequency inner race (Hz)
F_o	ball pass frequency outer race (Hz)
FTF	fundamental train frequency (Hz)
N	number of balls
n	speed (rpm)
B_d	ball diameter (mm)
P_d	pitch diameter (mm)
θ	contact angle (degree)

1. INTRODUCTION

The rolling bearing system is the essential element in the rotating machines. It is mainly used in many high-speed applications including aircraft engine bearings, turboshaft engines to low-speed applications including gearboxes and spindle units. Metal bearings are gradually replaced by thermoplastic bearings in different industries due to their high properties such as self-lubricating, improved toughness and excellent corrosion resistance. Moreover, they have many advantages such as silent operating transmission, improved resistance to corrosion and significant hardness.[1] In rolling bearings, the frequent repetitions of stress are concentrated in a very small volume of material which can cause rolling fatigue failure. Bearing failure can result in costly impacts on the whole machine.[2] The ability of FEM to identify the early failure state of a bearing is approved by comparison with experimental results of FFT velocity spectrums. Various topics of predictive maintenance have been studied to enhance understanding the bearing fatigue behavior. A part of them consists of assessing the evolution of the vibration response of bearing, to identify the mechanical condition of a bearing.

Computational analysis has been carried out in the past in the domain of fatigue behavior of bearings. The FE models are developed by applying explicit dynamic FE software in the past.[3,4] They apply an explicit-time integration method to evaluate acceleration, velocity, and displacement results.[5,6] Beyond implicit models,[7,8] explicit FE models of free defect bearings had been developed.[9–12] These studies evaluate the stress distribution within the ball bearings. The results of the rolling elements and raceways contact surfaces simulated by using FEA are compared with those of the classical Hertz theory of elasticity.[13,14]

Only a few studies had focused on modeling the vibration signals of defective bearings by means of an explicit FE software.[15–20]

Shao et al. proposed an optimization model of a ball bearing which has been solved by means of explicit LS-DYNA software.[17] It was considered that the bearing was mounted in a pedestal. Guochao et al. developed a 3D finite element model of a ball bearing with a localized outer race fault and showed that the ball bass frequency of the outer race F_o matches moderately well with the analytical results.[15] The outer race was modeled as a rigid. However, the material's behavior of the other components was not provided. Moreover, they didn't specify whether friction and damping were considered.

Liu et al. developed a 3D finite element model of a ball bearing which focuses on examining the impact of the localized faults forms on the vibration responses.[16] The different forms of localized faults were modeled on the outer races which are rectangular, hexagonal, and circular. It was mentioned that the simulated vibration and displacement responses were validated after comparing the numerical estimation of the outer race defect frequency to the analytical frequency. However, the simulated acceleration amplitude mismatched with experimental data which has been mentioned for many multi-body modeling results.[15,21–23] One possible explanation of the high amplitude may be the over-stiffening of the bearing and the nonlinear dynamics of rotor systems.[20] The FE model does not contain a shaft and therefore the center of the bearing model was hollow. Moreover, it was not shown whether damping and clearances was taken into account in the FE model.

Utpat proposed a 3D FE model of a defective bearing. The developed model was simulated by means of LS-DYNA.[19] He found that the vibration amplitude increased with fault size and rotating frequency. The obtained results agreed with experimental work.

Singh et al. modeled a 2D bearing composed of a line fragment on its outer raceway. The developed model was simulated by means of LS-DYNA.[18] The cited previous FE models modeled the entire outer race as rigid.[15,16,24] Singh et al. considered the whole bearing elements as flexible.[18] This assumption contributes to a lot of correct modeling of the bearing stiffness and therefore the vibration signatures. It was proved that the obtained vibration amplitude matches well with the experimental work. This validation was not approved in previous FE models and multi-body models.[15,16,19,21,23]

Singh et al. modeled contact forces between rolling elements and raceways.[25] This was neglected in other finite element models and multi-body approaches.[15–17,19,21,26] Thus, Singh et al. showed that when a ball hits the subsurface of a fault and produces lower acceleration amplitude, a higher acceleration signal is created once the balls are compressed between the contact surface of ball path.[18]

Sreenilayam-Raveendran et al. compared the performance of polyetheretherketone (PEEK) and polytetrafluoroethylene (PTFE) polymeric ball bearings to their steel counterparts.[27] Vibration analysis, operating frequency, and acoustic study were used to analyze the failure and the wear behavior of bearing. The experiments showed that the vibration signal of PEEK is lower than that of the PTFE ball bearing.

Recently, N. Gaaliche et al. investigated experimentally the impact of the location and size of the defects on the dynamic performance of ball bearings made of polyoxymethylene (POM) and polypropylene (PP).[28] Vibration responses of steel ball bearing were gathered using a piezoelectric accelerometer and compared to their plastic counterparts. The obtained results showed that metal and PP bearings reveal less vibration amplitude compared to that of POM. The overall vibration amplitude increases with the applied loading. These vibration responses are more pronounced in inner race defect compared to that in outer race defect.

Even though the previous studies had been performed on the simulation of vibration responses for metal bearings, only few experimental studies have been carried out to analyze the dynamic behavior of thermoplastic bearings.27,28

In this work, a rolling bearing system using the implicit finite element method is investigated to compute FFT spectrums of the vibration signals and the Von Mises stress distribution of thermoplastic bearing.

Hence, in-depth understanding of the dynamic performance of plastic bearings as well as a comparison with their metallic counterparts are carried out. Ball bearings made from PP material are tested and their vibration responses are compared with those for stainless steel bearings. The FEA is validated by an experimental study that uses an accelerometer to analyze the vibration signals after introduction of a fault on the inner ring and then on the outer ring of polypropylene bearings.

Traditionally, thermoplastics are modeled as linear elastic materials in FE analysis to reduce computational time. However, plastic shows a linear viscoelastic behavior at small applied strain and low operating temperature. Thus, the previous results obtained from the linear elastic analysis certainly led to divergences from reality. Therefore, this 3D model has adopted viscoelasticity to simulate the deformable rings of thermoplastic bearing. In addition, the thermal effect that is highly affected by the lubrification condition is considered in the material's model which is neglected in other models.[29] Thus, many mechanical considerations are modeled in this simulation which are generally not taken into account in previous studies. Friction, transfer path, clearance and damping viscosity are considered in the present work. For this purpose, this numerical dynamic simulation overcomes the difficulties encountered by previous studies to solve vibration and stress responses for the entire components of rotor by modeling the dynamic behavior of the rolling contacts and the flexibility of the races.

2. BEARINGS

The bearings used in the current investigation were manufactured from molded cylindrical bars made from Polypropylene (PP) shaft. Seven spherical roller balls made from glass were placed in the cage (see Fig. 1). The measurement of the bearings was taken from SKF 629 series, which is a deep groove radial-ball bearing. A similar bearing made from high carbon chromium was tested to compare its dynamic performance with its polypropylene counterpart. The mechanical properties of the selected bearing materials are provided in Table 1. Table 2 shows the dimensions of the specimens.

3. EXPERIMENTAL SET-UP AND INSTRUMENTATION

The developed fatigue test rig as shown in Fig. 2 was composed of a HP motor able to reach a maximum rotational speed

Table 1. Mechanical properties of polypropylene, glass and metal.[30]

Material	Modulus of elasticity (MPa)	Elongation at break (%)	Tensile Modulus (MPa)	Surface hardness'	Heat Deflection Temperature (○ C)	Coefficient of thermal expansion (10-6 × ○ C-1)	Poisson's ratio	Density (g/cm^3)
Polypropylene (PP)	12	600	402	R R 85	103	200	0.90	0.90
Glass	72000	-	70000	6 (Moh scale)	-	-	2.899	0.23
High carbon chromium (SUJ2)	$1,570$ to $1,960$	0.5 Max.	208	HB 650 to 740	200	12.5	-	7.83

Table 2. Dimensions of the test bearing.

Bearing Dimensions	Value
Outside diameter, D	26 mm
Bore diameter, d	9 mm
Width, w	8 mm
Ball diameter, Bd	4.762 mm
Number of balls, N	7
Pitch diameter, Pd	18 mm
Internal Radial Clearance	6 μm

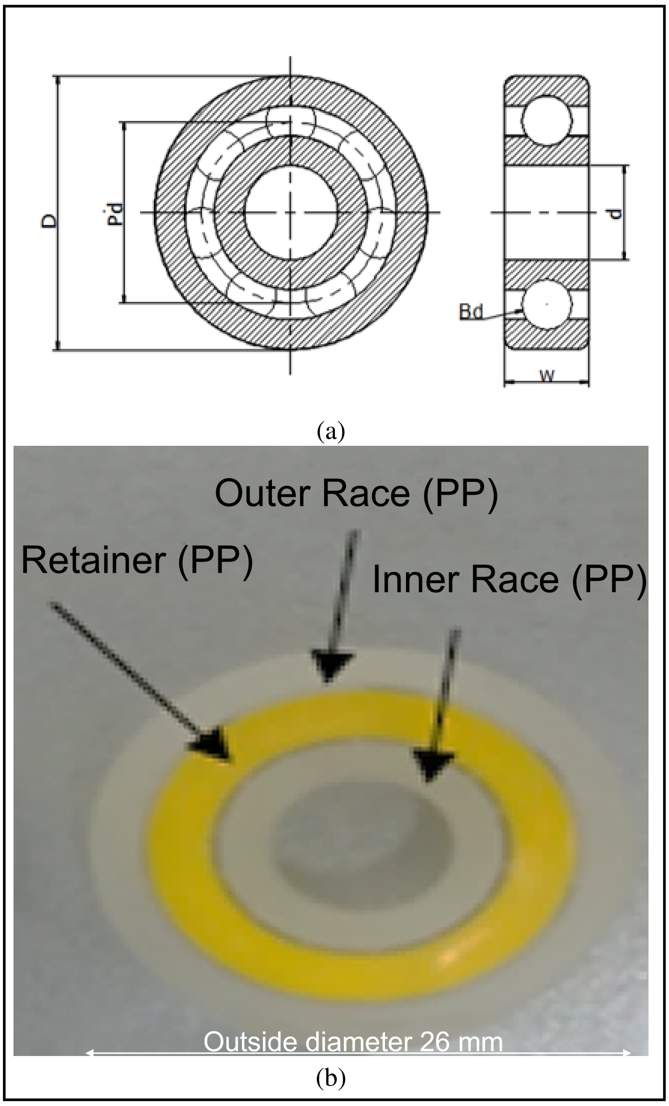

Figure 1. Test bearings. (a) The dimensional characteristics of bearings, (b) different materials of PP bearing parts.

of 1500 rpm by means of speed drive. The test rig was comprised of a shaft with a length of 45 mm and a diameter of 9 mm. A variable speed drive was used to adjust the motor speeds and to perform the test under different rotational frequencies. Loading was accomplished via a dead weight attached to the longer arm of 175 mm and varied to provide the specific applied load (Fig. 2). The vibration signals were gathered continuously using a piezoelectric accelerometer (see

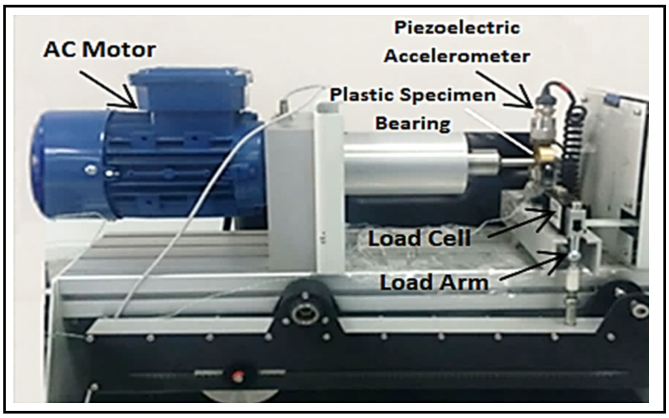

Figure 2. Fatigue test rig.[34]

Fig. 2). This accelerometer of sensitivity of 5 mV/g was fixed to the surface of the bearing housing via a magnetic base. This piezoelectric accelerometer was linked to the FFT analyzer that was connected to a data acquisition system. The vibration signals were processed and analyzed by ONEPROD xpr-300 software at a sampling rate of 102.4 kHz. The signals were processed offline (of 0.5 -second duration). This experimental apparatus was reported in paper.[28]

4. FINITE ELEMENT (FE) MODELLING FOR VIBRATION ANALYSIS OF THE ROLLING BEARING SYSTEM

The dynamic characteristics of the rotor at a speed of 1500 rpm and carrying a dead weight of 5N connected to its inner race were investigated using finite element analysis. The bearing was made of polypropylene and consisted of 7 glass balls as shown in Fig. 1. The polypropylene was modeled as a linear viscoelastic material using Multibody Dynamic Interface analysis. All components of the bearing were assumed to be flexible with the balls that were modeled as rigid bodies being exceptions. A retainer is used to maintain the rollers constrained in the inner and outer raceways. After the contacts, boundary conditions, Physics- Controlled Mesh Refinement controls and generalized alpha time-dependent solver controls were set, the model was solved and the results were examined. The analysis of the bearings with respect to the location of the defects were also investigated.

The geometry of the bearings with outer and inner race defects was modeled in CAD by Autodesk Inventor 2020 and shown in Fig. 3. The introduced faults were modeled by holes with a diameter of 1 mm. The developed model was subjected to Finite Element Analysis using the software Comsol Multiphysics 5.6. The geometry of ball bearing type varied as follows: outer and inner race defective bearings (Fig. 3).

The 3D model of the rolling bearing system is shown in Fig. 4. The CAD model was developed for a rotor bearing system including bearing, shaft, and housing. The three-dimensional model of the Rotor, shaft and housing was developed as per dimensions. The length of the shaft was 45 mm and both rings were tightly mounted on shaft and housing of

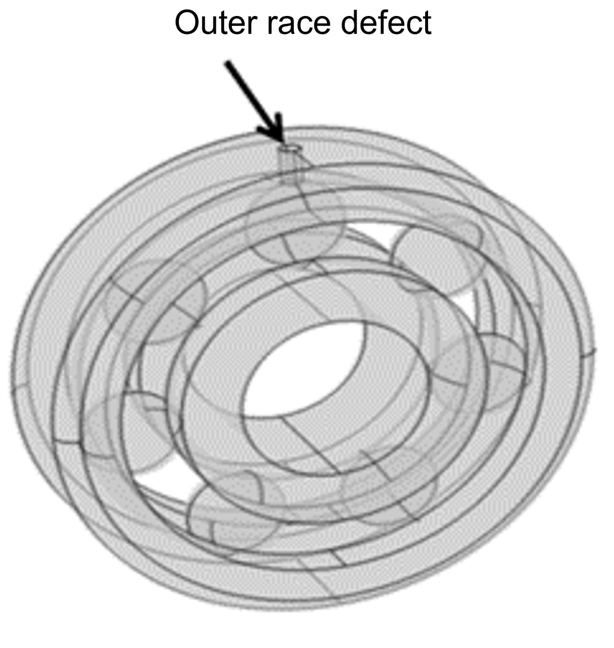

(a)

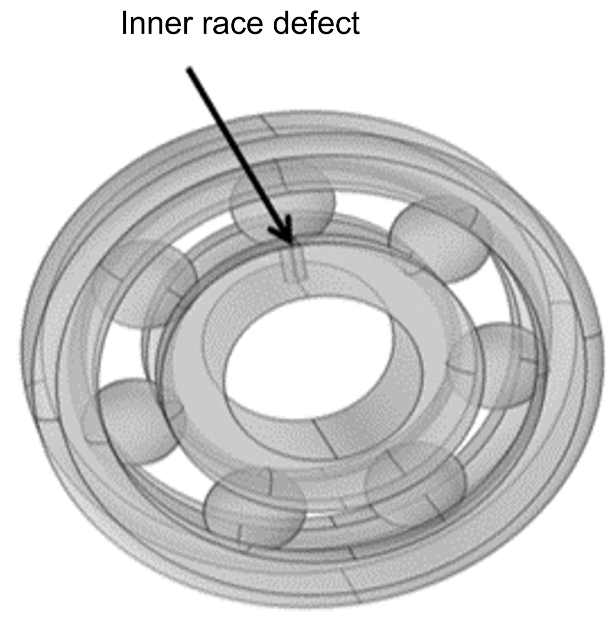

(b)

Figure 3. Geometry of ball bearings with defects of 1 mm diameter in (a) outer and (b) inner races models realized by Autodesk Inventor.

the rotor. In the pre-processing step, Young Modulus, Poisson's ratio, coefficient of thermal expansion and density of every part of the bearing were provided. The mechanical properties shown in Table 1 is provided as an input to the FEM analysis. In this numerical investigation, a 3D model of a ball bearing with stationary outer ring and rotating inner race was considered. Moreover, the flexibility of rings was considered and whether damping viscosity could be controlled. The standard gravity was also considered in this FE model. The necessary following details are provided to define the developed model.

PP was modeled as linear viscoelastic material with specific mechanical properties using Comsol Multiphysics (Table 1). It was also assumed that the polypropylene material had Bulk modulus "K" of 4 GPa and Shear Modulus "G" of 105.78 MPa. It's used for the inner, outer races and retainer, in order to investigate the effect of the flexibility of the material on the vibration and deformation responses. However, the seven balls were made from glass material and assumed as an isotropic and linear-elastic material.

Table 3. Types of contact between different bearing elements.

Contact Area	Type of contact
Between balls and rings	Frictional contact (coefficient of friction = 0.125)
Between balls and cage	Hinge joint

The boundary conditions of this model were imposed to ensure an adequate homogeneity with the developed experimental apparatus. A radial load of 5 N was applied to the outer race respectively for PP bearing. Displacements were considered zero in x, y and z directions. To simulate the stationary outer ring, fixed axial rotation boundaries were used on the outer ring to represent the boundary conditions. The Rotating Frame is applied for the rotation of the inner ring from the Multibody Dynamic interface. This will rotate the shaft and inner race with rotor angular velocity of 1500 rad/s, as shown in Fig. 4.

The contact between balls and races is modeled as friction contact. The connections between the balls and the retainer were simplified using hinge joints. A normal radial internal clearance of $6\ \mu$ m between the balls and the outer race was imposed using clearance joint. Suggested interface settings for different elements of bearings used in the analysis are listed in Table 3.

This simulation was used to account and analyze the deformations and stresses of bearings through different studies including Eigen frequency, Frequency response, Time dependent response and FFT response. Thus, many mechanical considerations were treated in these simulations which were usually ignored or difficult to model in the previous studies.

The next stage of the pre-processing phase of FE analysis was to generate the appropriate mesh of each part. After developing the computational domain, the bearings were discretized into tetrahedral elements of 0.1 size for FE analysis by means of Comsol Multiphysics (see Fig. 4 b). The trimming option was used to increase the resolution the contact elements.

In this work, modal analysis based on stress estimation for this model was carried out. The modal solver computes the eigenfrequencies and natural mode shapes of the developed model. The resonant frequencies which could produce high vibration amplitudes were also identified.

5. CONVERGENCE STUDY

To check the accuracy of the computed maximum RMS vibration amplitudes, a convergence study was carried out for different cases by increasing the number of elements. Physics-controlled mesh options were applied to increase the number of elements. In this present convergence study, the number of elements varied from elements 3593 to 31029 elements and the converged values of RMS vibration amplitudes is shown in Fig. 5. It was observed that convergence was achieved when coarse mesh was selected. Thus, the proposed tetrahedral mesh is validated. Since, it satisfies a good compromise between precision of the numerical results and faster convergence. The meshed model of the different components of the rotor, shaft and housing) is shown in Fig. 4 b.

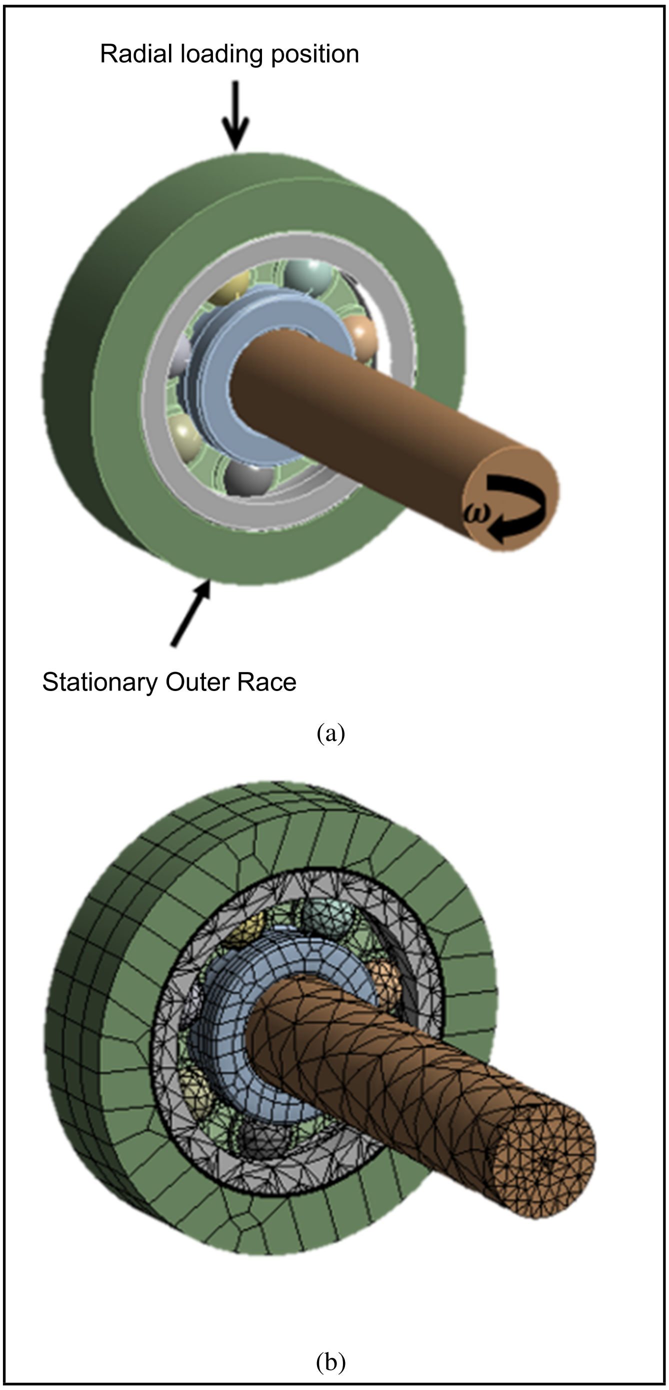

Figure 4. (a) FE model of the rotor, shaft and housing showing boundary condition and radial loading position– Comsol Multiphysics and (b) Meshed model with tetrahedral elements.

Table 4. Element size of the mesh and the total number of elements.

	Element size of the mesh	Number of finite elements
Physics-controlled mesh options	Extra coarse	3593
	Coarser	5399
	Coarse	11817
	Normal	17929
	Finer	31029

6. MODAL ANALYSIS

Modal analysis allowed for the determination of natural vibration frequencies and mode shapes. The different parts of the rolling bearing could be considered as a damping system. The following equation of motion of free vibration and undamped

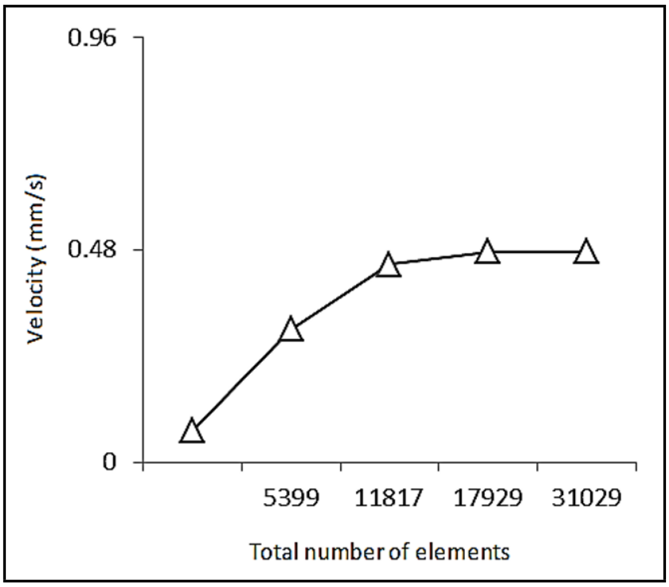

Figure 5. Convergence test results for velocity amplitude for the 3D model.

system is given below:[31]

$$[M]\{\ddot{X}\} + [K]\{X\} = \{0\}; \tag{1}$$

where $[M]$ was the mass matrix, $[K]$ was the stiffness matrix, $[\ddot{X}]$ was the acceleration vector, and $[X]$ was the displacement vector.

Based on the expression of the displacement vector $\{X\} = \{\phi\}\sin(\omega t + \varphi)$, the acceleration vector could be attained using the differential operators.

$$\{\ddot{X}\} = -\omega^2\{\phi\}\sin(\omega t + \varphi); \tag{2}$$

Therefore, the equation of the undamped system could be obtained by substituting the expressions of the acceleration vector and the displacement vector into the free vibration equation of motion.

$$([K] - \omega^2[M])\{\phi\} = \{0\}; \tag{3}$$

where ω was the characteristic root and $\{\phi\}$ is the characteristic vector.

The characteristic Eq. (3) was solved for the order of vibration ϕ, using non-linear modeling FE numerical approach. Figure 6 shows the shape modes of the rotor. The vibrations spread fully over the inner race in horizontal direction at modal frequencies of 3586 Hz and 8537 Hz respectively. Figure 7 depicts the simulation results of high vibration areas. At a natural frequency of 3586 Hz, the rotor and shaft bend and cause high vibration level (see Fig. 6 a). Figure 6 b depicts a severe inner race deformation at the natural frequency of 3586 Hz and 8537 Hz. Based on the modal analysis, natural vibration frequencies were determined which will indicate that, the RBR should not be operated at such speeds. The eigenfrequencies of the inner race were identified below 10 KHz. The order of the free vibration refers to the direction of movements, and the natural mode shapes were identified according to understanding. Figures 6 a and 6 b show the first and second modes of vibration of tested bearing.

7. PRINCIPLES AND INSTRUMENTS OF THE NATURAL FREQUENCIES' MEASUREMENT

To validate the obtained results of the developed FE model, an experimental modal analysis was carried out. Modal test-

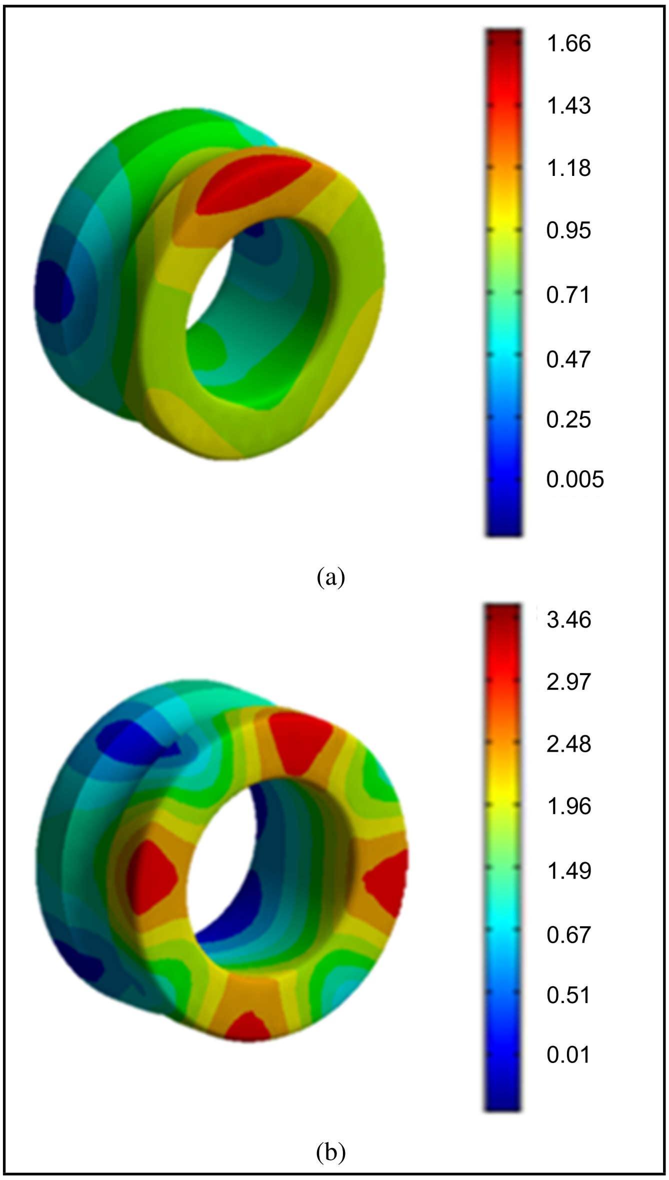

Figure 6. Inner Race vibrational deformation (mm). (a) Mode 1 frequency: 3586 Hz and (b) mode 2 frequency: 8537 Hz.

ing was a typical transient excitation that was used to excite the modal frequencies within a defined frequency range of the ball bearing using an impact hammer. This method was useful because the energy of an impulse response was distributed continuously within a frequency range. Processing the impulse excitation and measured response signals allowed for the determination of the Frequency Response Function (FRF) using FFT analysis of the tested bearing to determine its natural modal frequencies.

To conduct the modal impact test, the plastic bearing was hung freely with a flexible rope. The bearing under test was subjected to a light impulse excitation using the 8202-impact hammer from B&K company equipped with 8200 load cell sensitivity of 1.01 pC/N to determine the impulse response. The vibration responses were measured using the B&K 4384 accelerometer with a sensitivity of 0.810 mV/m/s^2 attached radially by wax on the outer ring of the bearing under test. Both force transducer and accelerometer were linked to a 3560 pulse multi-analyzer system which was connected to a 3022 four-channel input module and a 2825 acquisition front end from B&K company for further data processing of the frequency response function (FRF) up to 10 KHz. The schematic drawing

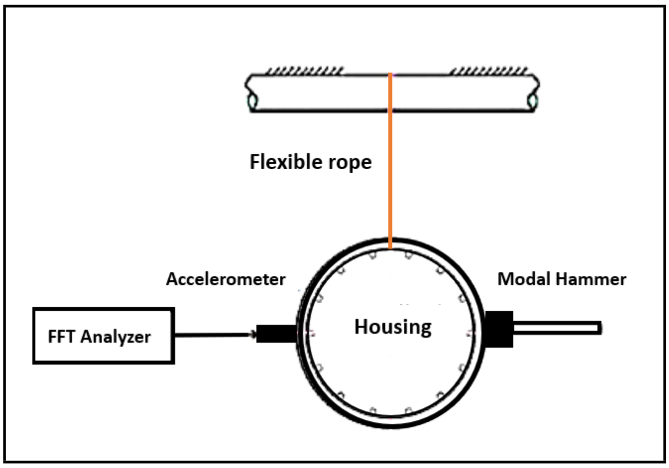

Figure 7. A schematic drawing of measuring system set up.

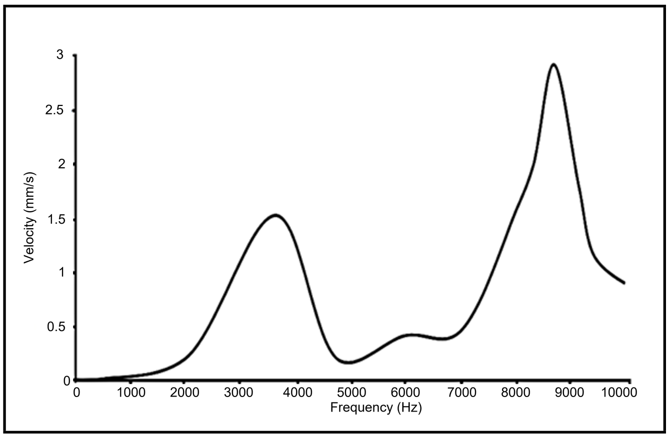

Figure 8. Frequency Response of tested thermoplastic bearing showing resonance frequencies at 3654 Hz and 8675 Hz.

of a measuring system of vibration modal analysis set up is shown in Fig. 7. The frequency response curve is displayed in Fig. 8 using Pulse LabShop software. The instrumental part includes the hammer, force transducer, the accelerometer and the FFT analyzer.

The comparison between the resonant frequencies obtained from the experimental measurements and the modal analysis through COMSOL MULTIPHYSICS are given in Table 5. The maximum relative errors were lower than 1.6 %. Moreover, the eigenfrequencies computed by modal analysis were lower than the measured results.

8. FREQUENCY RESPONSE

The characteristic defect frequencies were related to the rotational speed and the defect's location in a bearing. The repetition of the vibration signals of defects can be observed as peaks in the frequency spectrum. Pulses of very short durations were produced in a bearing due to the contact of defects and rolling elements during the rotating motion when the ball hits the fault. These pulses caused the excitation of the eigen frequencies of the different components of the bearing.

In the common case, where the outer race was stationary and the inner race is rotating, the characteristic defect frequencies

Table 5. Comparison between the model analysis results and the experimental measurements for the rolling bearing system.

Types of vibrations	Comsol Multiphysics	Measurement	Error
Mode 1 (Hz)	3586	3645	1.6
Mode 2 (Hz)	8537	8675	1.58

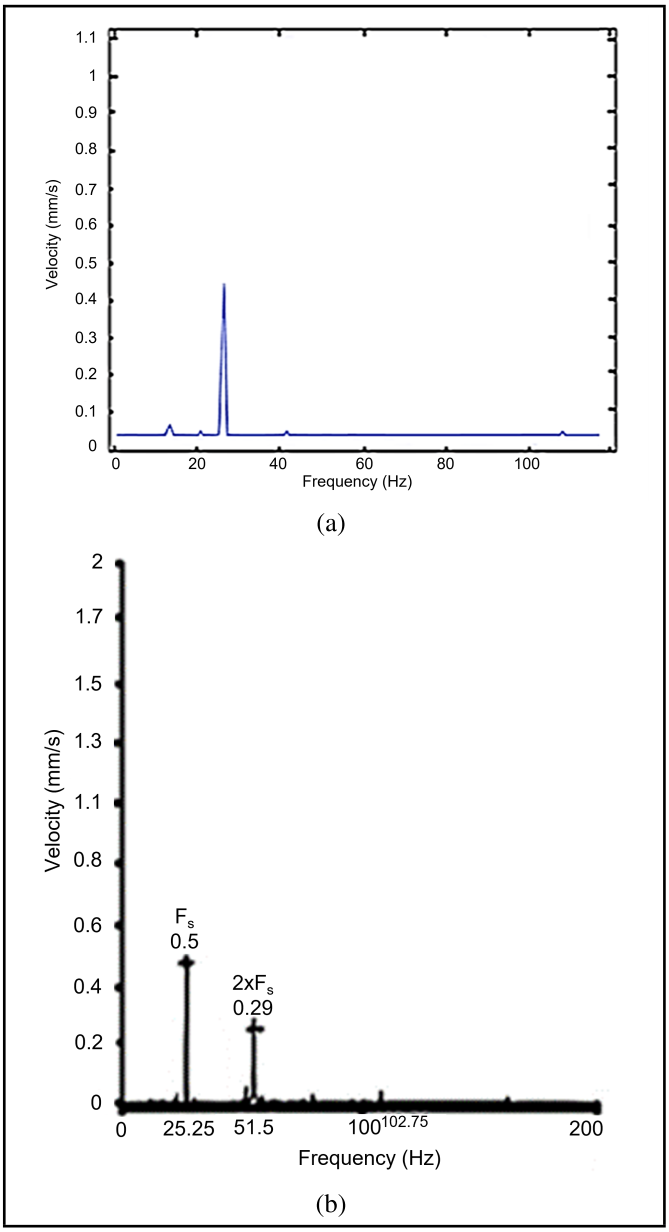

Figure 9. Simulated and Experimental Velocity Spectrums of defect free PP bearing for frequency 25 Hz at 5 N.

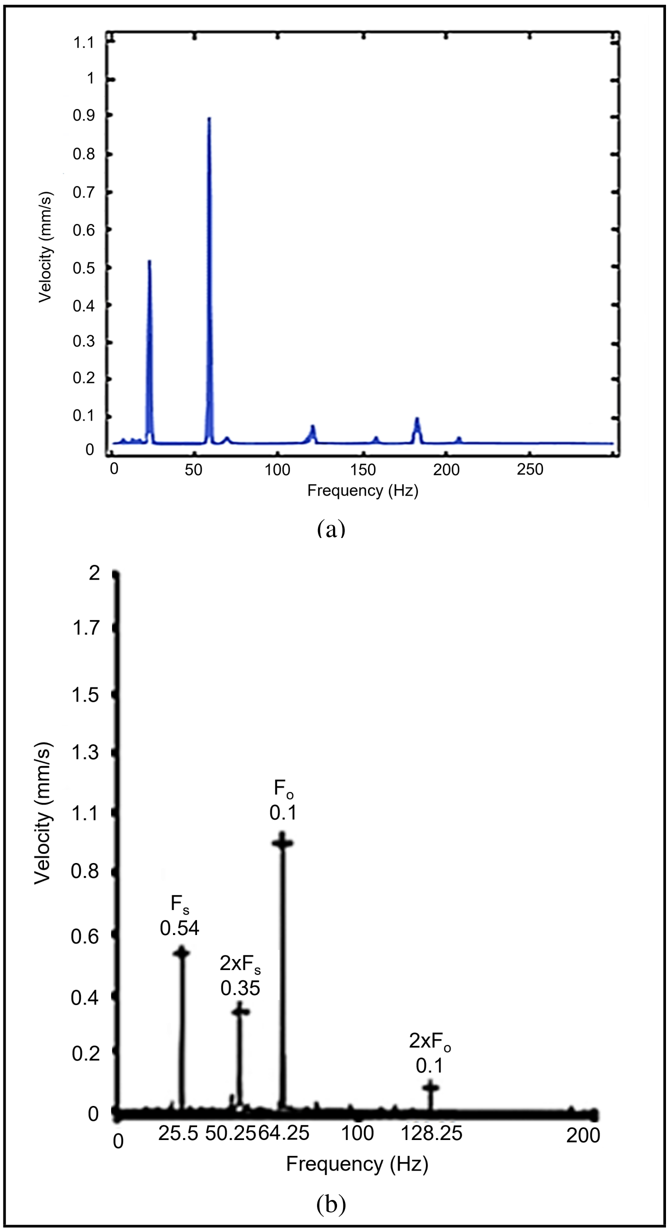

Figure 10. Simulated and Experimental Velocity Spectrums of 1mm outer race defect for polypropylene bearing for frequency 25 Hz at 5 N.

are given as follows:[32,33]

$$F_s = \frac{n}{60}; \tag{4}$$

$$F_o = \frac{N}{2} F_s \big(1 - \frac{B_d}{P_d} \cos\theta\big); \tag{5}$$

$$F_I = \frac{N}{2} F_s \big(1 + \frac{B_d}{P_d} \cos\theta\big); \tag{6}$$

$$FTF = \frac{F_s}{2} \big(1 - \frac{B_d}{P_d} \cos\theta\big); \tag{7}$$

where F_s was the shaft rotational frequency, F_I was the ball pass frequency inner race, F_o was the ball pass frequency outer race, FTF was the fundamental train frequency, N was the number of balls, n was the speed in rpm, B_d was the ball diameter, P_d was the pitch diameter, and θ was the contact angle.

A frequency-response analysis, which is the final step of vibration analysis, was used to compute the FFT dynamic response of the rolling bearing system subjected to rolling contact pulses that varied implicitly with time. Therefore, the FFT frequency analysis tool was used to determine the rotor response in a frequency domain. The radial load was 5 N for an operating speed of 1500 RPM. This force was applied in the radial direction to the housing as shown in Fig. 4.

The simulation results of the FFT frequency response of the ball bearing are shown in Fig. 9. Figure 9 a shows that large velocity amplitude occurs corresponding to the frequency of 25 Hz. Since 25 Hz is predominant, this corresponds to the shaft rotation frequency as shown in the Fig. 9 a. It can be observed that the rolling bearing system reaches a maximum of 0.47 mm.s-1. This result agrees well with the experimental RMS velocity level 0.5 mm.s-1 presented in the following Fig. 9 a. It can be clearly observed that the numerical F_s matches with the analytical one which is 25 Hz. The spectrums show the absence of peaks ranging within the characteristic defect frequencies which reveals that there is no fault existing in the tested bearing.[33] The FFT spectrums obtained from the FE simulations show less vibration peaks than the experiments. Since $2 \times F_s$ shaft rotation harmonic is observed only in the measured FFT response due to the rotor shaft misalignment.

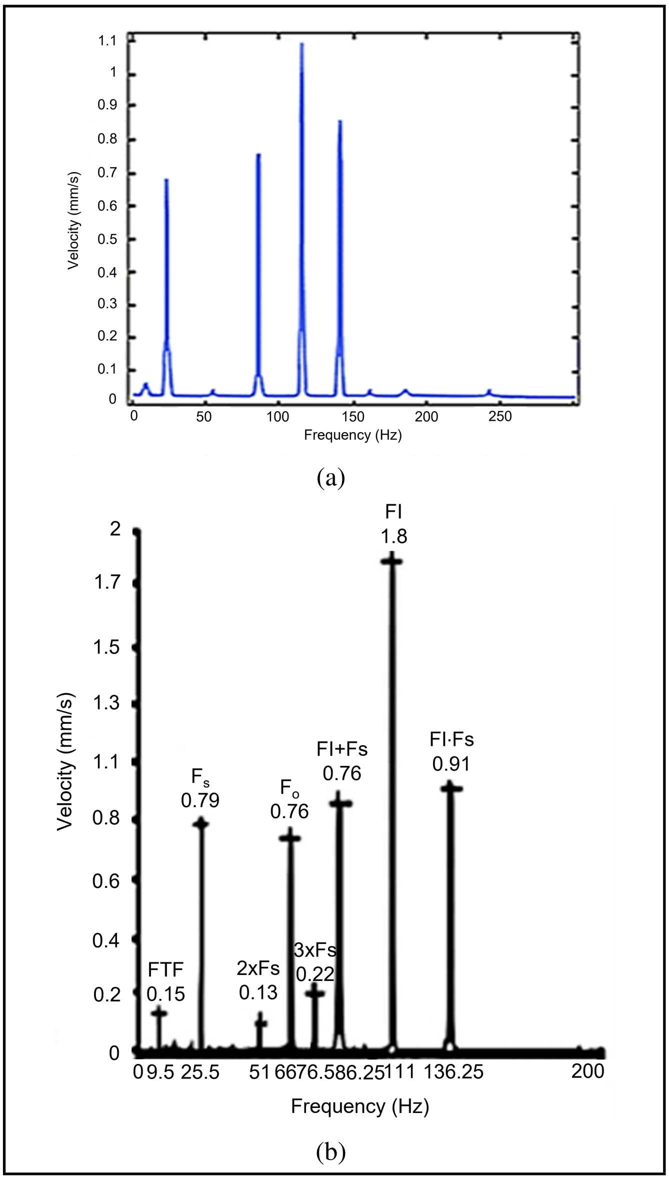

Figure 11. Simulated and Experimental Velocity Spectrums of 1 mm inner race defect for polypropylene bearing.

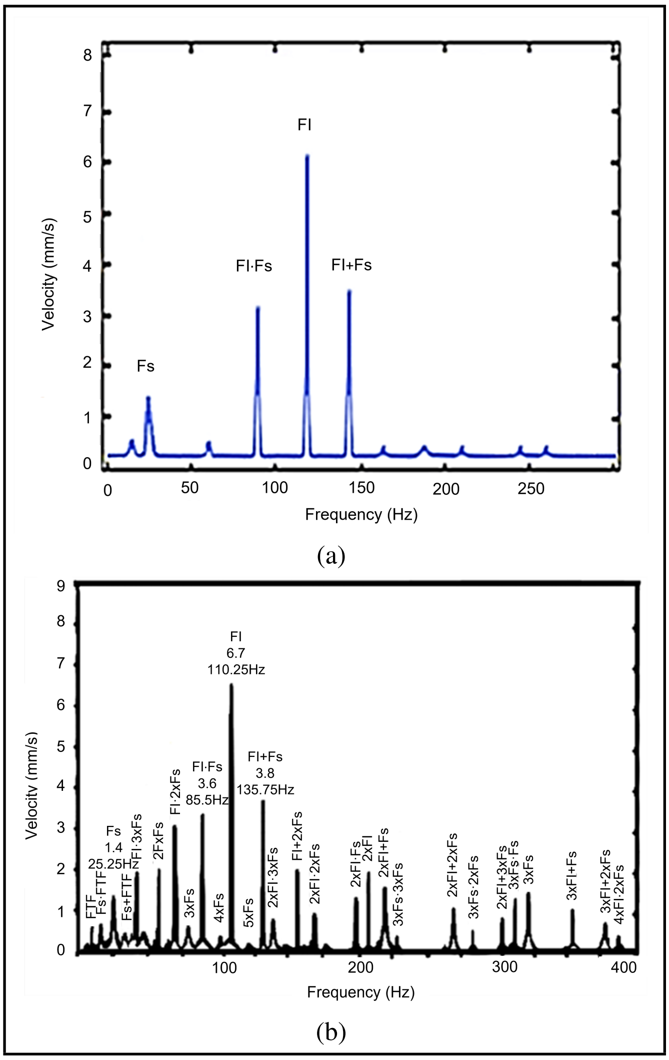

Figure 12. Velocity Spectrums of 1 mm inner race defect metal bearing for frequency 25 Hz at 5 N

Figure 10 b depicts the FFT vibration responses obtained from the FE simulation result of outer race defective PP bearings. It is obvious that the overall vibration amplitudes have been increased with the introduction of the defect. The FFT spectrum of the outer race defective bearing clearly shows the frequency of the outer race defect F_o calculated using Eq. (3) which is 64.35 Hz closely matches with the simulation defect frequencies Fo obtained from FEM analysis and the experimental results.[34]

A velocity spectrum of bearings of inner race defect with 1 mm is shown in Fig. 11 c. The Fast Fourier Transform spectrums are different to those obtained in outer race defective bearings. Figure 13 c shows peaks in the range of inner race defect frequency which is calculated using Eq. (6) 110.64 Hz and clearly indicates the presence of the defect present in the inner race of the bearing. Moreover, ball pass frequency inner race (F_I) is modulated with the shaft rotational frequency (F_s), which appears due to the unbalanced rolling elements caused by the looseness of the cage. Sideband frequencies are equal to $F_I \pm F_s$. The spectral data in Fig. 11 c with 1 mm inner race defect shows that the highest vibration amplitude observed at F_I was 1.1 mm.s-1. This feature correlates well with the experimental vibration amplitude which is 1.4 mm/s observed at F_I.[34] Both experimental and simulation results show that the PP bearings exhibit a trend of increasing overall amplitude with the introduction of the inner race defect.

In attempting to further comprehend the plastic bearing's behavior, both experimental and simulated vibration responses with their steel counterparts are investigated. The dynamic performance of the PP bearing and stainless-steel bearings are compared using the vibration spectrums for frequency 25 Hz at an applied load of 5 N. Figure 12 d shows the tested and simulated RMS velocity of the metallic bearing with an inner race defect of diameter 1 mm. As depicted in Fig. 12 d, a higher overall vibration level is observed in the metallic bearing, compared to that of PP bearing. For example, the velocity amplitude at F_I decreases from 6.7 mm/s to 1.94 mm/s for metal and PP bearings, respectively. The simulation results are in accordance with the experimental findings. A spectrum of steel bearing contains five harmonics of the shaft frequency $1 \times F_s$ until $5 \times F_s$ (Fig. 12 d) due to misalignment along with high vibration amplitude.[35] But, three shaft harmonics are observed in the spectrums of PP bearings (Fig. 11 c). This is due to the fact that plastic bearing compensates for shaft misalignments due to assembly imperfections.[36] Only one peak in the range of the inner race bearing defect frequency ($1 \times F_I$) was observed in the spectrum of polymer bearing (Fig. 11 c) compared to that of metallic bearing which contain up to $4 \times F_I$

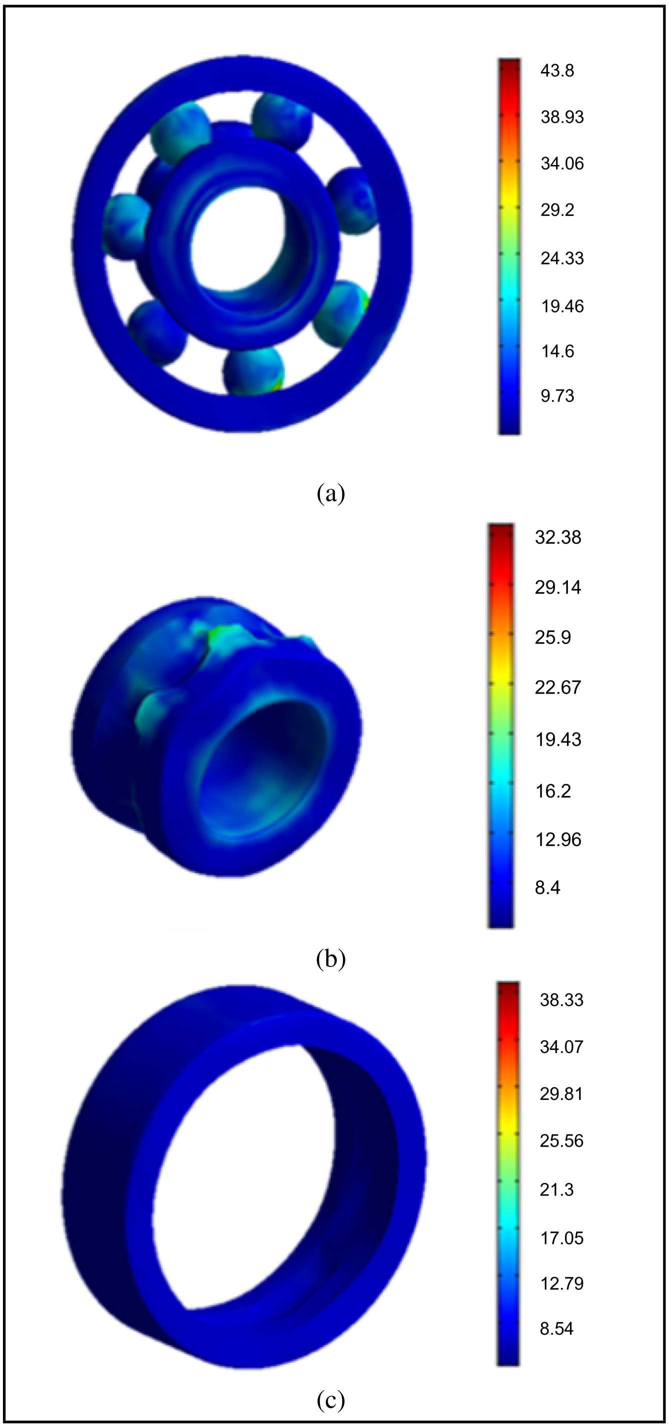

Figure 13. Ball bearing Von Mises stress. (a) Bearing (b) Inner race and (c) Outer race.

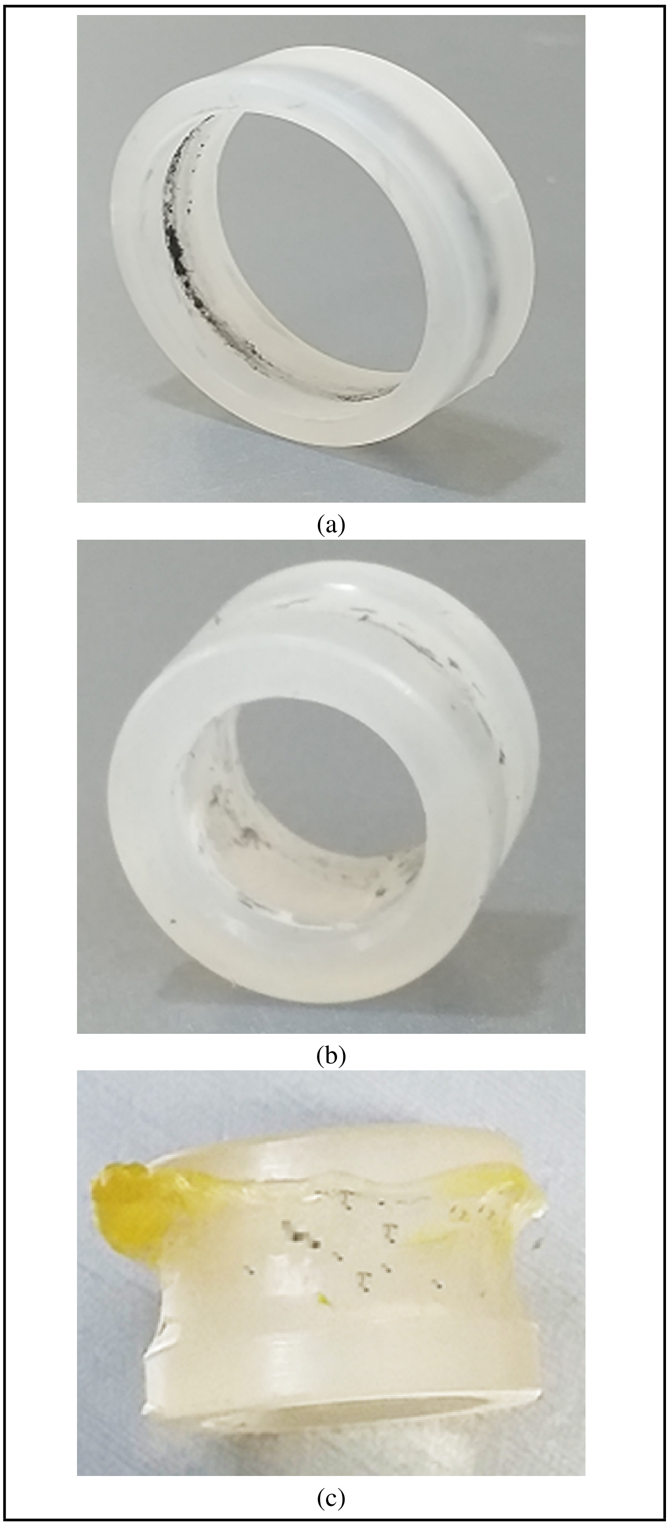

Figure 14. PP bearing after failure (a) Transfer film formation in the outer raceway, (b) Transfer film formation in the inner raceway and (c) Smeared area of melted retainer in the inner raceway.[28]

modulated by sidebands at $1 \times F_s$ (Fig. 12d), which can be explained using this feature. This is attributed to the fact that polymers are more effective at absorbing vibration than metals due to its greater damping capability.[37]

9. FAILURE SIMULATION

Figure 13 depicts the Von Mises stress distribution PP bearing under excessive loading conditions. The stress contour shows that the maximum peak stress is 38.9 MPa, and is found under the contact area near the rolling elements and rings. Its shape is deformed following the model of Hertzian contact theory (Fig. 13 a). The stress is mainly concentrated on the contact zone between the inner ring and rollers.[38–40]

The inner raceway surface is flattened by the glass rollers (Fig. 13 b). This simulation has been validated by Singh et. al.[18] They show that when a ball hits the subsurface of a fault and produces lower acceleration amplitude, a higher acceleration signal is created once the balls are compressed between the contact surface of ball path. These results are consistent with the experimental findings found, as they demonstrate that the self-adhered film is formed at the contact surface between glass rollers and PP inner race. It is a large thick adhesive film which is deposited on the race surface (Fig. 14 b).[28]

As shown in the Fig. 14 b, the plastic bearing expands thus the clearance between the shaft and the inner race is reduced due to the increase of the frictional heat, leading to additional wear. Thus, Fig. 14 c depicts black wear particles which are formed on the races of the bearing during the test. The PP transfer film including melted PP and graphite wear particles formed on the raceway are subjected to compression by glass rollers, and covered the whole race of the bearing. Under conditions of heavy loads smearing occurs, an accumulation of the melted retainer and races are formed on inner ring's path.[28] Figure 14 c shows a large, smeared area in the path of rolling elements which stops the bearing rotation. Then, the failure occurs, when the whole bearing assembly collapses.[41]

10. CONCLUSION

The effects of localized defect location on the vibration spectrums are investigated using the implicit Finite Element Method and experimental approach. The vibration responses of stainless-steel bearings are studied to compare the performance of the thermoplastic bearings with its metallic counterparts. The developed finite element model proves to be an efficient fault diagnostic approach to detect the defects in the plastic rolling bearing-rotor system and their severities. Based on the studies performed on dynamic response of the polymer bearings, it can be concluded that:

- The modal frequencies and natural mode shapes of the RBR have been computed by mean of the FE analysis. From the results, it can be seen that the two vibration modes corresponding to the PP bearing are respectively 3586 Hz and 8537 Hz, which cause high vibration.
- The FFT spectrum of outer race defective bearing clearly shows the frequency of outer race defect F_o which agrees well with the analytical results. The analytical verification depicts that the FFT spectrum of outer race defective bearing obtained through FEM analysis and FFT Analyzer are in accordance with the analytical one.
- A lower vibration level is observed in PP bearings compared to metal. The defect harmonics and sidebands are clearly identified in plastic bearing signatures when compared to those of metal. This can be contributed to the inherent ability of plastics to dampen vibrations and ensure silent operation compared to metals. This advantage results in less complexity in plastic bearing spectrums compared to those of metallic bearings.
- Von Mises stress simulations of PP bearing results show that the greatest stress distributions occur when the balls are compressed between the raceways. This observation allows predicting the fault area where a defect can appear causing premature failure.
- This 3D FE model considering the viscoelastic property, the flexibility and damping viscosity of thermoplastic can be used for any RBR system to carry out more realistic vibration analysis. This will allow to improve the design accuracy of the final product.

REFERENCES

[1] Glaeser, W. Polymeric Materials. *Materials for Tribology*, (20), 177–210, (1992). https://doi.org/10.1016/S0167-8922(08)70076-2

[2] Liu, J., Xu, Y., Pan, G. A combined acoustic and dynamic model of a defective ball bearing, *Journal of Sound and Vibration*, (501), 116029, (2021). 10.1016/j.jsv.2021.116029.

[3] *LS-DYNA Keyword User's Manual*, Livermore Software Technology Corporation, Vol.1., California, (2012).

[4] Ansys Autodyn, Release 14.5, Ansys Ip, Retrieved from http://www.ansys.com/Products/Simulation+Technology/Structural+Analysis/Explicit+Dynamics/ANSYS+Autodyn.

[5] Singh, S. *Explicit Dynamics Finite Element Modelling of Defective Rolling Element Bearings*, PhD Thesis, School of Mechanical Engineering, The University of Adelaide, South Australia 5005, Australia, (2014).

[6] Slack, S. and Sadeghi, F. Explicit finite element modeling of subsurface initiated spalling in rolling contacts, *Tribology International*, **43** (9), 1693–1702, (2010), https://doi.org/10.1016/j.triboint.2010.03.019

[7] Malhi, A. *Finite Element Modeling of Vibrations Caused by a Defect in the Outer Ring of a Ball Bearing*,Technical Report University of Massachusetts, USA, (2002).

[8] Rubio, H., Prada, J.C., Castejón, C. and Laniado, E. *Dynamic analysis of rolling bearing system using Lagrangian model vs FEM code*, The 12th IFToMMWorld Congress, Besancon, France, (2007).

[9] Fan, L., Tan, N. L., and Shen, D.P. FEA on stress field of rolling element bearing based on explicit dynamics, *Journal of Beijing Jiaotong University*, **30**(4) ,109–112, (2006).

[10] Lin, T. J., Rong, Q., Li, R.F. and Shao, Y. M, Finite element analysis for dynamic characteristic of a deep-groove ball bearing in motion process, *Journal of Vibration and Shock*, **28**(1), 118–122, (2009).

[11] Rong, Q., Lin, T. and Shao. Y. Finite element simulation of the motion process for deep-groove ball bearing, *Journal of Advanced Manufacturing Systems*, **7**(1), 9–13, (2008). https://doi.org/10.1142/S0219686708001024

[12] Zhang, Y., Xie, Y. Wu, X. and Lu, W. Finite element analysis for dynamic characteristic of deep-groove ball bearing operating from acceleration to constant speed, *Journal of North eastern University*, **33**(1), 103–107, (2012).

[13] Hertz, H. Überdie Berührungfesterelastischer Körper, On the contact of elastic solids, Reprinted in English Miscellaneous Papers by H.Hertz, (Eds.) Jones and Schott, London: Macmillan, 1896, *Journal of Reine and Angewandte Mathematik*, **92**, 156–171, (1882).

[14] Hertz, H. *Überdie Berührungfesterelastischer Körperandüberdie Harte, on the contact of rigid elastic solids and on hardness*, Reprinted in English Miscellaneous Papers by H.Hertz, Eds.Jones and Schott, London: Macmillan, Verhandlungendes Vereinszur Beförderungdes Gewerbefleisses, (1896).

[15] Guochao, L., Wei, P., Yongcai, L., Lixin, G., Zhang, J. Simulation and dynamic analysis of outer ring fault on rolling bearings using explicit finite element method, *China Mechanical Engineering*, **23**(23), 2825–2829, (2012). https://doi.org/10.3969/j.issn.1004-132X.2012.23.011

[16] Liu, J., Shao, Y. and Zuo, M.J. The effects of the shape of localized defect in ball bearings on the vibration waveform, *Proceedings of the Institution of Mechanical Engineers, Part K: Journal of Multi-body Dynamics*, **227**(3), 261–274, (2013). https://doi.org/10.1177/1464419313486102

[17] Shao, Y., Tu, W. and Gu, F. *A simulation study of defects in a rolling element bearing using FEA, International Conference on Control Automation and Systems*, Gyeonggi-do, Korea, 596–599, 2010.

[18] Singh, S., Köpke, U., Howard, C. and Petersen, D. Analyses of contact forces and vibration response for a defective rolling element bearing using an explicit dynamics finite element model, *Journal of Sound and Vibration*, **333**(21), 5356–5377, (2014). https://doi.org/10.1016/j.jsv.2014.05.011

[19] Utpat, A. Vibration signature analysis of defective deep groove ball bearings by numerical and experimental approach, *International Journal of Scientific and Engineering Research*, **4**(6), 592–598, (2013).

[20] Sharma, A.,Upadhyay, N., Kankar, P.K., Amarnath, M., Nonlinear dynamic investigations on rolling element bearings: A review, *Advances in Mechanical Engineering*, **10**(3), (2018), https://doi.org/10.1177/1687814018764148

[21] Patil, M.S., Mathew, J. Rajendrakumar, P.K. and Desai, S. A theoretical model to predict the effect of localized defect on vibrations associated with ball bearing, *International Journal of Mechanical Sciences*, **52**(9), 1193–1201, (2010). https://doi.org/10.1016/j.ijmecsci.2010.05.005

[22] Su, Y.T. and Lin, S.J., On initial fault detection of a tapered roller bearing: frequency domain analysis, *Journal of Sound and Vibration*, **155**(1), 75–84, (1992). https://doi.org/10.1016/0022-460X(92)90646-F

[23] Tandon, N. and Choudhury, A. An analytical model for the prediction of the vibration response of rolling element bearings due to a localized defect, *Journal of Sound and Vibration*, **205**(3), 275–292, (1997). https://doi.org/10.1006/jsvi.1997.1031

[24] Uluyol, O., Kim, K. and Hicken, b. C. Update to a Systematic Approach to Bearing Health Monitoring, 7th DSTO International Conference on Health & Usage Monitoring, Australia, (2011).

[25] Singh, S. Howard, C., Hansen, C. and Köpke, U. Numerical noise generation in modelled bearing vibration signals, Proceedings of Inter noise 2014, The 43rd International Congresson Noise Control Engineering, Melbourne,Victoria, Australia, (2014).

[26] Zhao, S., Liang, L., Xu, G., Wang, J. and Zhang, W. Quantitative diagnosis of a spall-like fault of a rolling element bearing by empirical mode decomposition and the approximate entropy method, *Mechanical Systems and Signal Processing*, **40**(1), 154–177, (2013). https://doi.org/10.1016/j.ymssp.2013.04.006

[27] Sreenilayam-Raveendran, K., Azarian, M. H., Morillo, C. M., Pecht, G., Kida, K., Santos, E. C., Honda, T. and Koike, H. Comparative Evaluation of Metal and Polymer Ball Bearings, *Wear*, **302**, 1499–1505, (2013). https://doi.org/10.1016/j.wear.2013.01.057

[28] Gaaliche, N., Chithambaram, S. Fathallah, R. Effect of defect size and load on the performance of thermoplastic bearings, *Journal of Testing and Evaluation*, **49**(5), (2020). https://doi.org/10.1520/JTE20190766

[29] Liu, J., Xu, Z. A simulation investigation of lubricating characteristics for a cylindrical roller bearing of a high-power gearbox, *Tribology International*, **167**, 107373, (2022). https://doi.org/10.1016/j.triboint.2021.107373

[30] HBOT3D, HBOT3D-Material-Catalogue-EN, Retrieved from https://hbot3d.com/wpcontent/uploads/2018/10/HBOT3D-Material-Catalogue-EN.pdf

[31] Shang, X. Qiu, F., Zhao, H. and Li, W. *Finite Element Senior Analysis Method for Structure with ANSYS and Application*. Beijing: China Waterpower Press, 119-126, (2008).

[32] Harris, T. A. *Rolling Bearing Analysis*, Third Edition, John Wiley & Sons, 672-673, (1991).

[33] White, G. *Introduction to Machine Vibration*, DLI Engineering Corp, (1997).

[34] Gaaliche, N., Chithambaram, S. Fathallah, R. Experimental investigations of dynamic performance of polypropylene ball bearings, *Journal of Theoretical and Applied Mechanics*, **50**, 20-35,(2020).

[35] Hujare, D., Karnik, M. Vibration responses of parallel misalignment in Al shaft rotor bearing system with rigid coupling, *Materials Today: Proceedings*, **5**(11), Part 3, 23863-23871, (2018). https://doi.org/10.1016/j.matpr.2018.10.178

[36] Plastic bearings excel in contaminated environments, MOTORS & DRIVES, Machine Design, (2000). https://www.machinedesign.com/motors-drives/article/21827875/plastic-bearings-excel-in-contaminated-environments

[37] Geethamma, V., Asaletha, R., Nandakumar, K., Thomas, S. Vibration and sound damping in polymers, Resonance **19**, 821-833, (2014). http://jtambg.eu/issues.php?year=2020&vol=50&issue=1

[38] Sharma, A., Amarnath, M., Kankar, P.K. Nonlinear dynamic analysis of defective rolling element bearing using Higuchi's fractal dimension. *Sādhanā*, **44**, 76 (2019). https://doi.org/10.1007/s12046-019-1060-x

[39] Sharma, A., Amarnath, M. Kankar, P.K. Effect of Varying the Number of Rollers on Dynamics of a Cylindrical Roller Bearing, Proceedings of the ASME 2014 International Design Engineering Technical Conferences and Computers and Information in Engineering Conference, Volume 8: 26th Conference on Mechanical Vibration and Noise. Buffalo, New York, USA. August 17–20, 2014. V008T11A067. ASME. https://doi.org/10.1115/DETC2014-34824

[40] Sharma A., Amarnath M. Kankar P.K. Effect of Unbalanced Rotor on the Dynamics of Cylindrical Roller Bearings. In: Pennacchi P. (eds) Proceedings of the 9th IFToMM International Conference on Rotor Dynamics. Mechanisms and Machine Science, vol 21. Springer, Cham. https://doi.org/10.1007/978-3-319-06590-8_136

[41] Marshek, K. M. Failures in Plastic Ball Bearings, *Wear*, https://doi.org/52,141 – 146, (1979).